

A Single Motor Mobile Robot with Passive wheels: A propulsion mechanism and a robotic realization

Satoshi Ito¹, Kosuke Niwa², Shoya Sugiura³, and Ryosuke Morita⁴

Abstract—This study proposes a passive-wheeled mobile robot that propels itself with a single motor. Its propulsion principle is basically the same as that of a snakeboard: maintain the symmetrical orientation in the front and rear wheels and drive the rotor to obtain propulsive force. This process is rhythmically and alternatively repeated between the left and right directions. A feature of mechanism is that the single motor driving the rotor is fixed with an allowance to the body. Utilizing the rotation caused by this allowance, the wheel orientations are switched until the limiter positions. The propulsion mechanism is tested using an actual robot. The effect of the rotor weight and spring attachments is also experimentally investigated.

I. INTRODUCTION

Recently, most city environments are paved, and slopes are built between each building floor. In such a barrier-free flat ground, wheeled systems have an advantage in maneuvering. Among various wheeled systems, passive wheels are widely utilized because they can be realized by merely attaching casters to their bottom. Passive wheel systems can be categorized into two types: 1) dolly-type systems, which are used by pushing or pulling and have a propulsion that completely depends on the *assistive* force generated by user and 2) the roller-skate type, in which the passive wheel systems can move autonomously and have some degrees of freedom (DoF) of motion other than the wheels that contribute to drive themselves indirectly.

The latter passive wheel mechanism is more convenient to use because no external assistive forces are required. Instead of external assistive forces, some propulsive forces must be created using other mechanisms equipped on the passive wheels [1], [2], [3]. Currently, low DoFs are preferable for the force creation because they need less actuators with large weight and high cost. This study aims at propelling a passive-wheeled robot imitating a two-wheeled snakeboard (Fig. 1) or the snakeboard mechanism with only a single actuator. The snakeboard robot normally possesses three actuators: two for the orientation adjustment of the front and rear wheels and one for the rotor rotation [4], [5].

We previously proposed a robot that moves like a snakeboard with a single actuator [6]. However, this robot required

a special key device, namely a torque limiter, for its construction. A torque limiter is a mechanical device that disconnects the torque transmission when a large torque is applied. This device is difficult to design and manufacture by ourselves, reducing the facilitation of manufacturing the whole robot. The friction-based function of the torque limiter produces wearings that never ease the control because of nonlinearity or degradation. The torque limiter removal is preferable from the viewpoint of manufacturing and controlling.

Accordingly, we propose herein a new propulsion mechanism comprising more general mechanical parts such as gears and bearings that can be easily obtained. Compared to [6], the contribution of this paper is the construction of a new propulsion mechanism without a torque limiter. A mathematical model was established in our unpublished paper [7]. This paper experimentally investigates robot behaviors for the propulsion, the load effect on the rotor and the spring attachment. In particular, a model with spring will be newly proposed.

II. DESIGN AND MANUFACTURING

A. Problem

The proposed mechanism aims at motions similar to those of a snakeboard (Fig. 2).

As the first step for propelling a passive-wheeled board by a single motor, all the DoFs, except for the passive wheel rolling (i.e., wheel orientation and rotor rotation), must be coupled to transfer the force from the motor.

The wheel orientations in normal snakeboard motions can be symmetrical in the front and the rear: the rear wheel faces angle α to the right when the front wheel faces angle α to the left. This kind of symmetrical rotation can be achieved by engaging two similar gears.

Herein, the problem is the coupling between the wheel orientation and rotor rotation caused by the following inconsistent requirements in the usage of these DoFs. The basic principle of the snakeboard progression is as follows: restrict the progress direction by maintaining the wheel orientation, and drive the rotor to obtain the propelling force by its counter force. A snakeboard achieves progression by repeating this principle in the right and left alternatively. In this process, the wheel orientation should be kept “constant”, while the rotor must be “accelerated/decelerated” to obtain the counter force.

The ways to satisfy these two contradicting requirements become a key for the robot structure design.

¹Faculty of Engineering, Gifu University, Yanagido 1-1, Gifu 501-1193, Japan satoshi@gifu-u.ac.jp

²Graduate school of Engineering, Gifu University, Yanagido 1-1, Gifu 501-1193, Japan v3038000@edu.gifu-u.ac.jp

³Graduate School of Natural Science and Technology, Gifu University, Yanagido 1-1, Gifu 501-1193, Japan x4525046@edu.gifu-u.ac.jp

⁴Faculty of Engineering, Gifu University, Yanagido 1-1, Gifu 501-1193, Japan rmorita@gifu-u.ac.jp



Fig. 1. A two-wheeled skateboard.

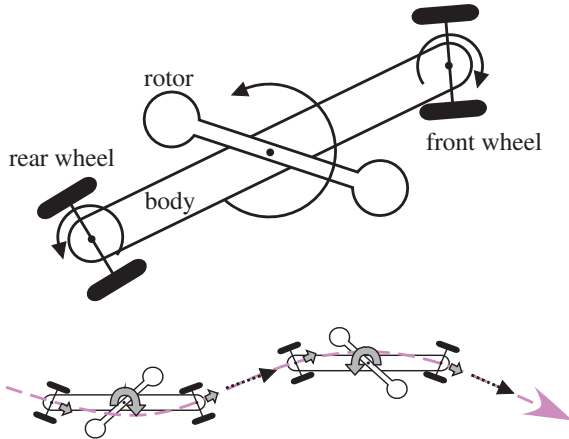


Fig. 2. A snakeboard and its progression.

B. Solution

The motor was attached to the rotor to coincide in their rotation axis. The motor was then normally fixed completely to the board's body to rotate the rotor.

However, in this study, the actuator was fixed with a given allowance; hence, it had room to rotate itself by the counter force of the rotor rotation.

More precisely, the motor was fixed to the motor support (Fig. 3), and this motor support was designed to rotate in some ranges with respect to the board's body. The wheel orientations were coupled to be changed by the motor support rotation (Figs. 4(a) and (b)).

In the robot design, the moment of inertia of the rotor should be set larger than that of the motor support to effectively obtain the counter force. In particular, when the motor was driven, the part that started the rotation was not the rotor, but the motor support. If the motor support continues to rotate forever, the board will never run because the motor output is consumed only in this motor support rotation. Thus, the limiter is introduced to restrict the range of the motor support rotation (Fig. 4(c)). This limiter defines the angle of the wheel orientation mechanically because the rotation in the wheel orientation is coupled to the motor support.

The actual rotation of the rotor starts when the limiter restricts the rotation of the motor support: the limiter catches the counter force of the rotor rotation, and the force received by the limiter becomes the propelling force for the board itself.

C. Robot design

Fig. 5 depicts the designed robot comprising four wheels: the front and rear wheels were coupled in its orientation

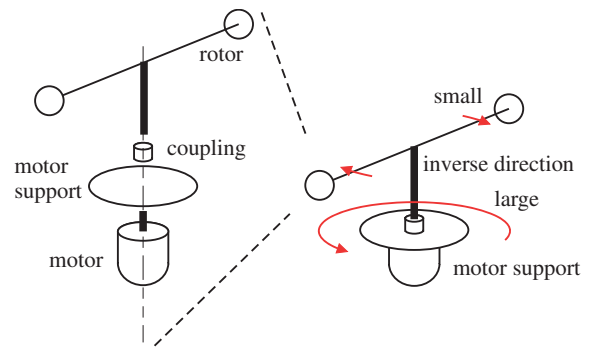


Fig. 3. Motor support.

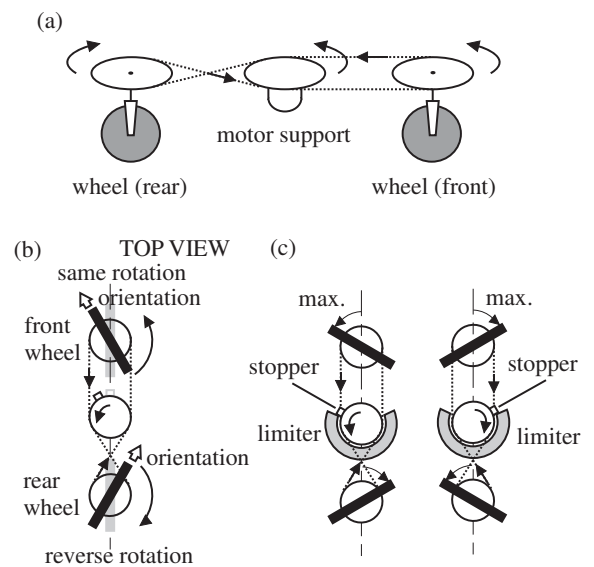


Fig. 4. Coupling of motor support to the rotation of the wheel orientation.

axis with the motor support rotation, while the two omnidirectional wheels were for the side supports. Spherical wheels were adopted to the front and rear wheels to reduce the friction in changing its orientation. Combining the gears and the timing belts, the rotation of the front wheel orientation was the same and that of rear wheel was opposite to the direction of the motor support. The limiter was installed at the rotation axis of the front wheel orientations. The orientation angle was designed to change the range from $-\pi/6$ to $\pi/6$. Two weights were placed at both tips of the rotor to gain the moment of inertia. The table on the rotor allowed this robot to convey some small baggage.

D. Manufactured robot

Figure 6 shows the completed robot comprising the length of 380 mm, width of 370 mm, height of 183 mm, and weight of 3.3 kg. A 20 W DC motor with gears in a 128:1 ratio was installed. The rotary encoder equipped in the motor can detect the motor angle deviation.

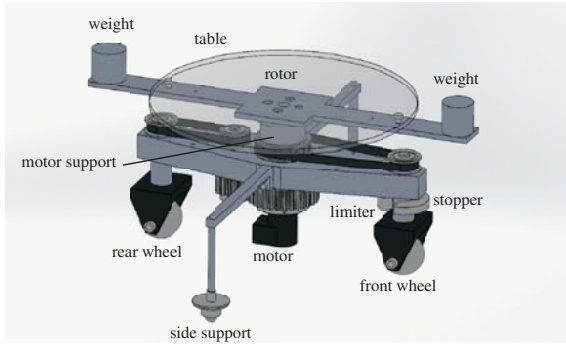


Fig. 5. Designed robot.



Fig. 6. An actual manufactured robot.

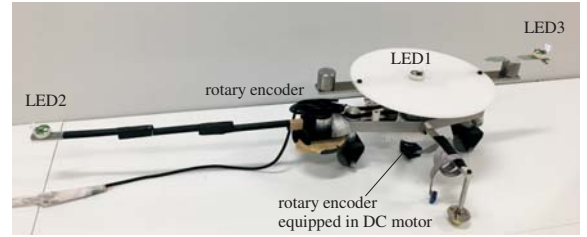


Fig. 7. Marker position for the motion capture system

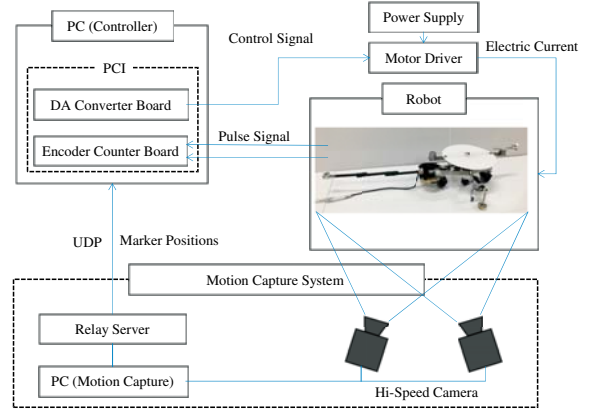


Fig. 8. Experimental setup



Fig. 9. Snapshots during an experiment.

III. EXPERIMENTS

A. Objectives

This section describes the experiments that were conducted using the robot as described in the previous section. The objectives of the experiments were to confirm the following:

- whether the mechanism proposed in this paper can actually propel the robot, even with only a single actuator, as expected
- whether a payload placed on the table can improve the distance traveled by increasing the moment of inertia, and
- whether a spring around the rotor axis of rotation enhances the efficiency.

These objectives are investigated in each sections below.

B. Experimental setup

A personal computer running ART-Linux was used as the controller for the robot. The output from the rotary encoder incorporated into the DC motor of the robot was connected to an encoder board (Interface PCI-6201) installed in this computer. To detect the wheel orientation, another encoder (Autonics E40HB), attached to the rotation axis of the rear wheel, was also connected to this board.

The torque computed by this computer was converted to an analog control signal for the motor driver (TITech Robot

Driver PC-0121-1) using an AD converter board (Interface PCI-3120) in the computer. The motor driver output drives the robot's motor using the external power supply.

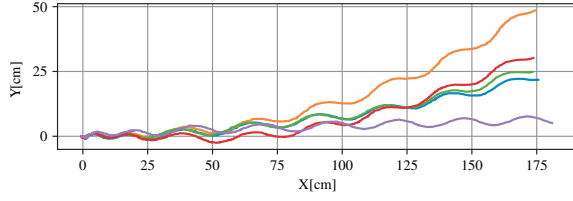
In addition, to measure the robot position in the workspace, a motion capture system (Library Radish) was introduced. This motion capture system features two high-speed cameras (Library GE60) operating at 50 Hz, and the measured positions of the markers were sent to the controller by means of UDP communication via a relay server. Three LEDs were attached to the robot center (the center of the rotor rotation), the tip of the tail extending from the main body and one of the rotor tips, as shown in Fig. 7. This tail part made from ABS material, which was not installed in Fig. 6, is light in weight, 35g, in comparison with the body. Thus we did not consider that it affected the experimental results such as the traveling distance.

The controller operated at 1000 Hz and, for safety, the output torque was restricted to the range ± 4.97 Nm by the code of control. For the control, the position control

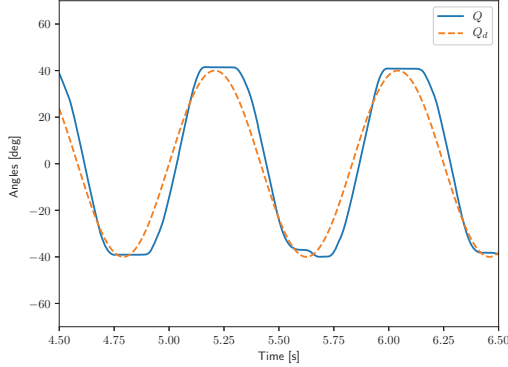
$$\tau = K(Q_d - Q) \quad (1)$$

is adopted, where τ is the motor torque, Q is the motor (rotor) angle, and Q_d is its desired position. K is the position gain, and it was set to 0.2 throughout the experiments.

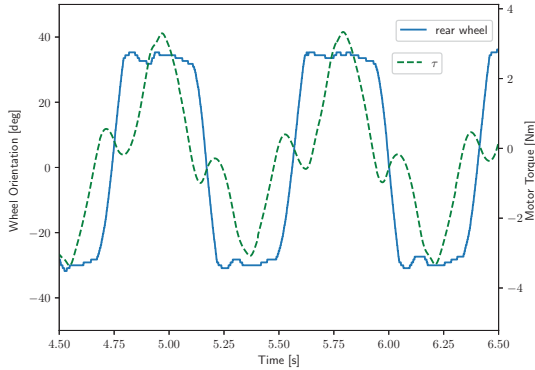
The overall experimental setup is summarized in Fig. 8.



(a) Robot center orbits for each of five trials



(b) Rotor angle and desired position during one experiment



(c) Motor torque and rear wheel orientation during one experiment

Fig. 10. Results of the propulsion experiment

C. Propulsion

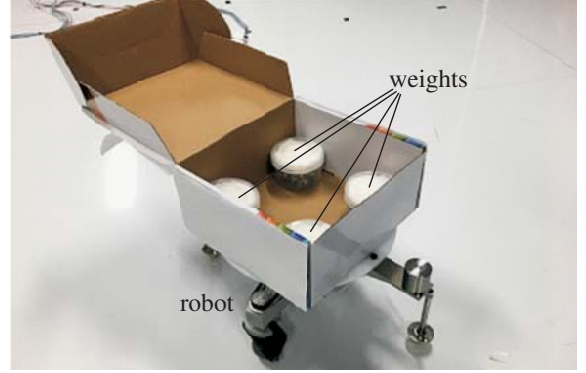
1) *Conditions:* We simulated the robot making forward progress as a result of the sinusoidal rotor motion [8]. Thus, the desired sinusoidal position change is given to the position controller:

$$Q_d = A \sin 2\pi f t \quad (2)$$

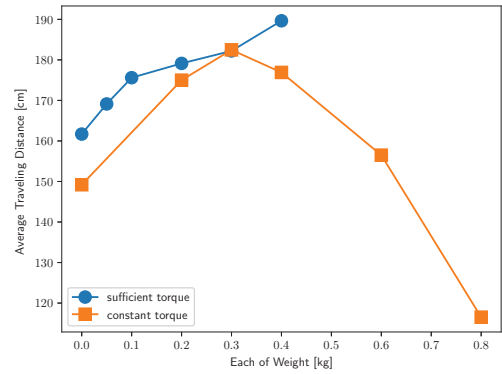
In the experiment, we set $A = 40^\circ$ and $f = 1.2$ Hz. The 7-s trials were conducted five times, starting from the same initial conditions in each case.

2) *Results:* The orbits of the robot center relative to the start position are shown in Fig. 10(a). The robot was able to propel itself even though a fluctuation in the forward direction was observed during the trials.

Figure 10(b) shows the time course of the motor angle Q and its desired position Q_d . The rotor angle followed the desired position although some delay is observed.



(a) Weights on the table of the robot



(b) Distance of travel vs. weight load

Fig. 11. Results of the weight effect experiment

Figure 10(c) shows the time course of the rear wheel orientation and the motor torque τ . The square-shaped graph of the rear wheel orientation indicates that the wheel orientations alternate between -30° and 30° , as expected. The change in the wheel orientation starts when the direction of the rotor torque changes. After the wheel orientation has flipped, the torque value becomes a maximum. That is, the counter torque effectively propels the main body while maintaining the wheel orientations.

D. Weight Load

1) *Conditions:* A table could be attached to the rotor of the robot. Placing a payload on the table will usually reduce the acceleration because of the increase in the total weight, but it also increases the moment of inertia of the rotor, resulting in the generation of a large counter force. Therefore, we set out to determine whether there are any cases in which the robot travels faster or farther if a weight is placed on the table.

To determine this, the experiments were conducted with some weights placed on the table. As shown in Fig. 11(a), four identical weights were aligned with the corners of a square cardboard box on the table. The 6-s experiment was conducted three times, with changing each of the weights from 0 to 0.05, 0.1, 0.2, 0.3, and 0.4 kg. The desired position is given as (2), with $A = 30^\circ$ and $f = 1.2$ Hz. The average

distance of travel was determined for the three trials.

2) *Results:* The circle plots in Fig. 11(b) correspond to the results representing the distance of travel versus the weight on the table. This clearly shows that, as the weight increases, the robot travels farther. That is, the weight increases the moment of inertia of the rotor, which enhances the propulsion produced by the counter force of the rotor rotation.

This result is, however, within a range limited by the maximum output of the motor. An excessive amount of weight, which exceeds the capacity of the motor, could be placed on the table. To investigate this, we conducted further experiments in which we maintained a constant torque. That is, the motor torque, which is sinusoidal, is defined as

$$\tau = A_\tau \sin 2\pi ft \quad (3)$$

where $A_\tau = 3.0$ Nm and $f = 1.2$ Hz. The 6-s experiment was conducted three times, with the weight being changed from 0 to 0.2, 0.3, 0.4, 0.6, and 0.8 kg in each trial.

The average distance of travel for the three trials is depicted by the square plots in Fig. 11(b). A smaller weight reduces the distance of travel because there is less counter force. An excessively large weight also reduces the distance of travel because there is insufficient motor power to spin the rotor sufficiently. The optimal value depends on the rotor design, in that if the rotor is lighter, the robot motion can be optimized when a predefined load to convey is placed on the table.

E. Spring Attachment

1) *Conditions:* Sinusoidal motion requires a motor to consume energy since it is not a constant-speed rotation but rather a frequent reversing motion. Basically, the sinusoidal motion appears as a harmonic oscillation in a passive system with a mass and a spring. Thus, the introduction of mechanical springs to help the rotor oscillation would be expected to reduce the energy consumption of the motor because the energy is stored in the deformed springs.

To explore this possibility, two springs with a stiffness of 0.26 N/mm were installed around the rotor, as shown in Fig. 12(a). The rotor was mounted on a new coupling which was attached to the motor axis. Because a thrust bearing was incorporated into the new coupling, the rotor spins without constraints around the motor axis. The spring was placed between this coupling and the rotor to limit rotor spins and store the energy.

In the first experiment, the desired position is given as (2), for which $A = 30^\circ$ and $f = 0.6$ Hz. The 8-second experiment was repeated five times. In the second experiment, the torque was directly set as a sinusoidal signal by (3) for the robot with and without spring. Three frequencies, $f = 0.6, 0.8$ and 1 Hz, were tested with keeping $A_\tau = 3.0$. The 5-second experiment was conducted three times for each condition and the traveling distance was measured.

2) *Results:* All the five trials in the first experiment drove the robot more than 150cm though some variations were observed. Figure 12(b) shows the time course of the traveling distance to the forward direction for one of the five

trials: an experiment conducted without the springs, under the conditions $A = 30^\circ$ and $f = 0.8$ Hz in the previous experiment, is indicated by the dashed line. Although the data are not shown here, the robot moved at most 10 cm even at $f = 0.8$ Hz without the springs: the traveling distance will be shorter at lower frequency $f = 0.6$ Hz (we had confirmed the higher frequency brought the robot farther in other experiments). On the other hand, it is drastically extended by the presence of the springs.

Figure 12(c) shows the time course of the motor angle and rotor angle. The motor angle follows the desired trajectory both with and without the springs. However, the rotor angle differs greatly. The rotor angle is the same as the motor angle in the experiment without the springs (indicated by the dashed line). On the other hand, the rotor angle measured using the motion capture system shows a large oscillation with an amplitude of more than 150° . This allows the robot to move forward even when there is only a small oscillation in the motor angle.

Figure 12(d) shows the time course of the motor torque. Although we expected that the spring would reduce the torque more, about double the torque was generated in the motor to cope with the reaction force from the springs. However, the traveling distance increased more than 10 times. Considering these scaling factors, we can say that the spring effectively stores energy during the rotor oscillations and makes the best use of that energy for forward progression.

In the first experiment, the motor motion was set to the same as shown in the green and blue line in Figure 12(c). However, the torque output might be different. Thus, in the second experiment, the equivalent sinusoidal torque was outputted for with and without spring conditions. Because the robot did not always go straight, the distance between the start and the final position was measured. The results was shown in Figure 13. The spring prolonged the traveling distance about 1.5 times when the frequency was 0.8 Hz or 1.0 Hz. This result also indicates that the springs will improve the energy efficiency of this type of robot.

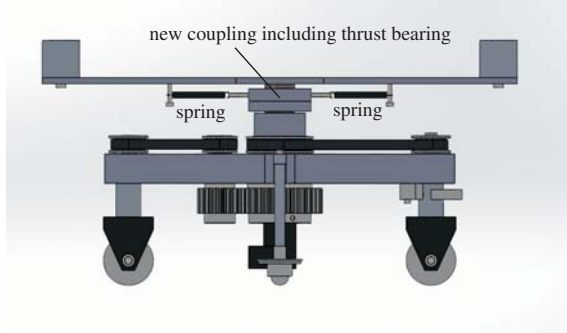
F. Simulation of spring effect

We have already proposed a mathematical model of this type of robot [7]. Here, we develop it to include the spring dynamics, as shown in Figure 14.

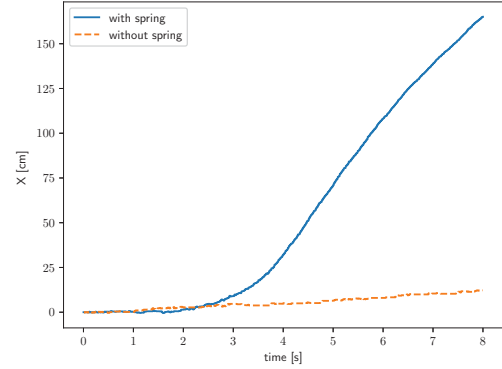
The model in Figure 14 has a planner dynamics with non-holonomic constraints driven by the counter force of the rotor motion τ_0 . The difference from the previous paper [7], and the key of the modeling, is the dynamical connection around the motor support. The three angles are introduced: the angle of the motor support including the motor itself relative to the robot's main body θ_{sp} , the motor angle based on the motor support θ_m , and the rotor angle relative to the motor angle θ_R .

The rotor is connected via the SPRING introduced in the section III-E. Approximating this effect by a 'torsion spring' with stiffness k_{spring} , the dynamics of the rotor is given as:

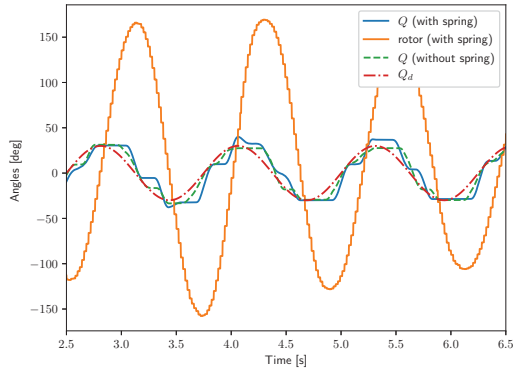
$$I_R \ddot{\theta}_R = k_{spring}(\theta_m - \theta_R) + b_R(\dot{\theta}_m - \dot{\theta}_R) \quad (4)$$



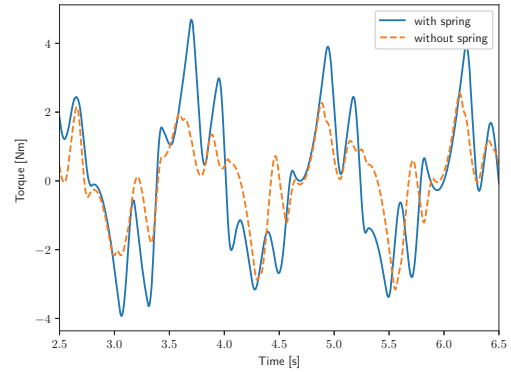
(a) Spring attachment



(b) Effect of spring on traveling distance



(c) Effect of spring on angle deviation



(d) Effect of spring on motor torque

Fig. 12. Results of the weight effect experiment

$$I_m \ddot{\theta}_m = -k_{spring}(\theta_m - \theta_R) - b_R(\dot{\theta}_m - \dot{\theta}_R) + \tau \quad (5)$$

Here, I_R and I_m are the moment of inertia of the rotor and the motor axis including the thrust gear, respectively, b_R is the viscous coefficient of the thrust gear and τ is the torque of the motor corresponding to the control input.

The motor support also rotates according to the counter torque $-\tau$. This dynamics is given as:

$$I_{sp} \ddot{\theta}_{sp} = -\tau - b_{sp} \dot{\theta}_{sp} + \tau_L \quad (6)$$

where b_{sp} denotes the viscous friction coefficient of the motor support rotation. This rotation is, however, restricted by the mechanical limiter, whose function is modeled with the high stiffness spring k_L and the high viscous damper b_L : The force (torque) from the spring-damper system restricts the movable range of the motor support, which is described as follows:

$$\tau_L = \begin{cases} -b_L \dot{\theta}_{sp} + k_L(\theta_{L+} - \theta_{sp}) & (\theta_{sp} > \theta_{L+}) \\ 0 & (\theta_{L-} < \theta_{sp} < \theta_{L+}) \\ -b_L \dot{\theta}_{sp} + k_L(\theta_{L-} - \theta_{sp}) & (\theta_{sp} < \theta_{L-}) \end{cases} \quad (7)$$

where θ_{L-} and θ_{L+} define the allowance of the motor support rotation.

Finally, the counter torque $-\tau_L$ drives the main body of the robot, i.e., $\tau_0 = -\tau_L$.

The simulation aiming at reproducing Figure 13 resulted in Figure 15. The parameters there were $K_{spring} = 0.5$ and $B_R = 0.02$. The case without spring was simulated using the high-stiffness spring $k_{spring} = 50$. Although the control laws were different, i.e., (3) in Figure 13 whereas (1) in Figure 15, the similar tendencies were obtained. To fit the experimental data well, the adjustment or identification on parameters are required more. Then the simulations will be utilized to evaluate the energy efficiency by the spring attachment.

IV. CONCLUSION

This paper proposed a new wheeled robot mechanism resembling the two-wheeled skateboard, or the snakeboard, that can progress autonomously with using only the single motor. The propulsion principle is confirmed by the actual motions of the robot. Furthermore, experiments demonstrated that, when the robot carries a payload, the weight of that payload can be utilized to increase the moment of inertia of the rotor to enhance the propulsion force, and the provision of springs around the rotor may allow the robot to make greater progress than that which is possible with no springs attached.

Recently, we have found that this robot curves by adding the increasing/decreasing offset to the sinusoidal input for the

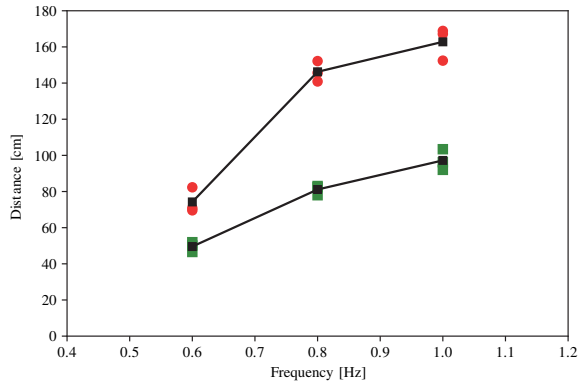


Fig. 13. Traveling distance comparison between with (red) and without (green) spring for the same sinusoidal torque. The black dots denote the average of three data.

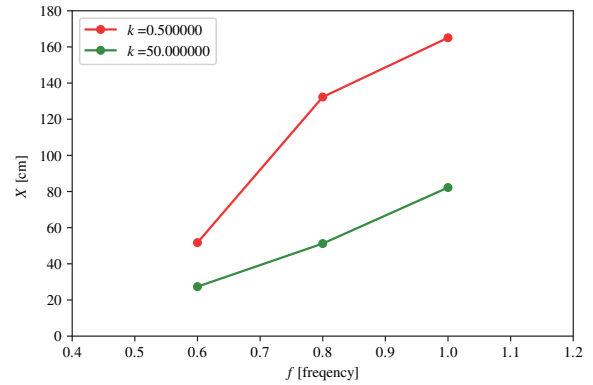


Fig. 15. Simulation considering the spring.

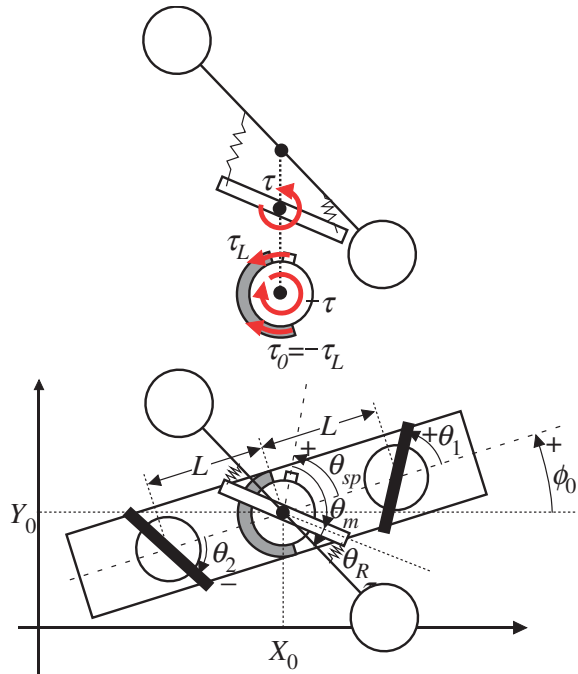


Fig. 14. Mechanical model of the one-actuator robot we proposed.

rotor rotations (see the movie). However, we found by some pilot experiments that the curving motions was difficult to achieve when the springs were installed. As the future work, we are aiming at the navigation of this robot to the goal position, utilizing the curving movements, with incorporating the spring mechanism.

A part of this paper is supported by ‘Human resource development and research project on production technology for aerospace industry : Subsidy from Gifu Prefecture’.

REFERENCES

- [1] P. Krishnaprasad and D. P. Tsakiris, “Oscillations, se(2)-snakes and motion control,” in *Proceedings of the 34th IEEE Conference on Decision and Control*, vol. 3. IEEE, 1995, pp. 2806–2811.
- [2] F. Bullo and M. Zefran, “On mechanical control systems with non-holonomic constraints and symmetries,” *Systems and Control Letters*, vol. 45, no. 2, pp. 133–144, 2002.
- [3] S. Hirose and H. Yamada, “Snake-like robots [tutorial],” *IEEE Robotics & Automation Magazine*, vol. 16, no. 1, pp. 88–98, 2009.
- [4] J. Ostrowski and J. Burdick, “The geometric mechanics of undulatory robotic locomotion,” *The international journal of robotics research*, vol. 17, no. 7, pp. 683–701, 1998.
- [5] S. Iannitti and K. Lynch, “Minimum control-switch motions for the snakeboard: A case study in kinematically controllable underactuated systems,” *IEEE Transactions on Robotics*, vol. 20, no. 6, pp. 994–1006, 2004.
- [6] S. Ito, S. Sugiura, Y. Masuda, S. Nohara, and R. Morita, “Mechanism and control of a one-actuator mobile robot incorporating a torque limiter,” *Journal of Intelligent & Robotic Systems*, 2019 (Accepted) DIO: 10.1007/s10846-019-01036-8.
- [7] S. Ito, S. Nohara, Y. Masuda, J. Yabuki, and R. Morita, “An autonomous mobile robot with passive wheels propelled by a single motor,” *Robotics and Autonomous Systems*, vol. 122, 2019 (Accepted) DIO: 10.1016/j.robot.2019.103310.
- [8] S. Ito, S. Takeuchi, and M. Sasaki, “Motion measurement of a two-wheeled skateboard and its dynamical simulation,” *Applied Mathematical Modelling*, vol. 36, no. 5, pp. 2178–2191, 2012.